



This manuscript is a non-peer reviewed preprint submitted to EarthArXiv. An open access, peer-reviewed version of this article is now available at Volcanica:

<https://www.jvolcanica.org/ojs/index.php/volcanica/article/view/218>,

<https://doi.org/10.30909/vol.06.02.405413>. Please refer to that instead of this pre-print.

SilicH₂O: a graphical user interface for processing silicate glass Raman spectra and quantifying H₂O

 T. D. van Gerve^{*α} and  O. Namur^α

^α Department of Earth and Environmental sciences, KU Leuven, Belgium.

ABSTRACT

H₂O contents of magmas strongly impact the explosivity of volcanic eruptions, as well as their rheological properties and crystallisation behaviour. Accurate analyses of H₂O in magmatic liquids are therefore vital for our understanding of the dynamics of magmatic processes and eruptions. Raman spectroscopy provides an accessible, affordable and high spatial resolution technique for estimating H₂O contents of magmas that have been quenched to a glass during eruption. However, calculating H₂O concentrations from Raman spectra involves manual data processing and results are therefore sensitive to the specific treatment used. SilicH₂O is an open-source software program that uniformises and streamlines this process by providing an interactive graphical user-interface. It can be used to: (a) process Raman spectra of silicate glasses, (b) remove any unwanted peaks through interpolation and unmixing, (c) set up H₂O calibrations with reference materials and (d) quantify H₂O contents of unknown samples.

KEYWORDS: Raman spectroscopy; Glass; Hydrous melt; Software; Python.

1 INTRODUCTION

Knowing the H₂O contents of magmas is crucial for understanding their phase equilibria, crystallisation behaviour, physical properties and eventual eruption style. However, traditional methods to measure H₂O in volcanic glasses, such as secondary ion mass spectrometry (SIMS) and fourier transform infrared (FTIR) spectroscopy, can be expensive and require extensive sample preparation. In contrast, confocal Raman spectroscopy is affordable, requires little preparation and has similarly high spatial resolution, but requires (often) complicated post-processing of collected spectra. The most important processing step is removal of background signal, for which different authors use different algorithms, producing different results. Moreover, the tools used for processing are not always made publicly available and the ones that are typically rely on code (e.g. Python, Matlab) that users have to implement themselves (e.g. Le Losq et al. 2012; Di Genova et al. 2017). SilicH₂O is an open-source software program that streamlines and uniformises post-processing of Raman spectra by providing an intuitive graphical user interface (Figure 1). It is aimed at quantifying H₂O in silicate glasses of any composition and integrates tools for unwanted peak removal, background subtraction and H₂O calibration. Results produced with SilicH₂O indicate that with the implemented data processing algorithms

H₂O can be measured by Raman spectroscopy with accuracies and precisions of mostly below 0.1 wt.%. 30

This manuscript introduces the main concepts of silicate glass Raman spectroscopy and its H₂O calibration and reviews the most important features of SilicH₂O (version 1.0.0). The software is available for Mac and Windows and can be downloaded from GitHub[†], with step by step installation and usage instructions available in its documentation[‡]. 35

2 RAMAN SPECTROSCOPY

Raman spectroscopy is based on the analysis of inelastically scattered light inside solids, liquids and gasses (Raman 1928; Frezzotti et al. 2012; Pasteris and Beyssac 2020). In a Raman spectroscope, a monochromatic laser is focused on a sample, exciting the vibrations of molecular bonds within the sample. This transfer of energy between the incoming laser's photons and molecular vibrations inelastically scatters the outgoing photons causing shifts in their vibration frequency and these shifts are then measured in wavenumber units (cm⁻¹). Raman shifted frequencies depend on molecular composition and vibrational mode (stretching or bending), while the scattered light intensity is (amongst other things; e.g. acquisition parameters) proportional to concentration of chemical species (Neuville et al. 2014; Malfait 2018). As such, Raman spectra of scat- 40 45 50 55

*  thomas.vangerve@kuleuven.be

[†]<https://github.com/TDGerve/silicH2O>

[‡]<https://silich2o.readthedocs.io/en/latest/>

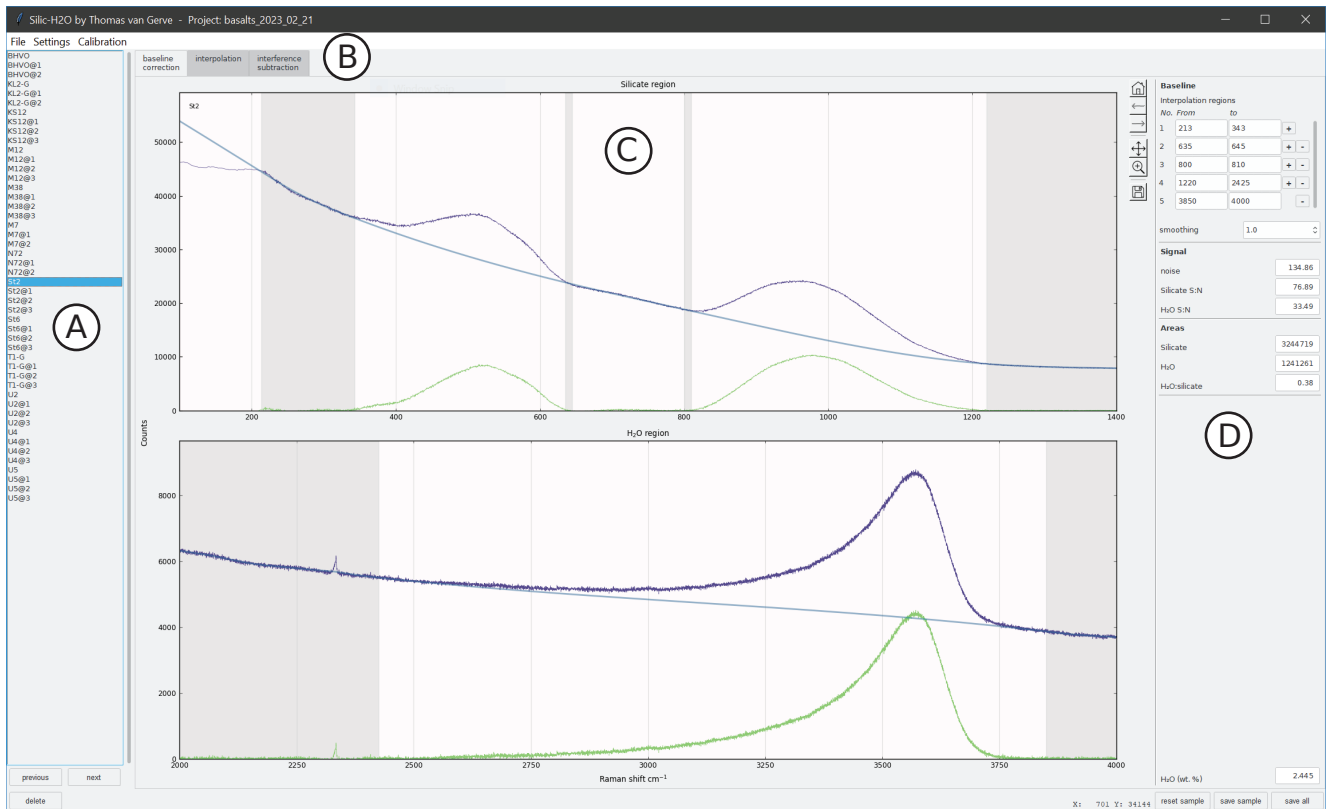


Figure 1: The main user interface of SilicH₂O (running on Windows OS), with **A** sample selection bar, **B** tool selection bar, **C** interactive spectrum with baseline interpolation regions as grey bars and **D** settings and results bar.

tered light intensities as a function of their frequencies offer qualitative information on both the structure and composition of analysed samples.

2.1 Analytical considerations

The focus of this paper is on measuring H₂O in glasses. Some care has to be taken during analyses, as glasses heat up due to partial absorption of the laser light. In opaque glasses, such as glasses with high iron contents or nanoscale crystals, this may lead to water loss or even melting (Behrens et al. 2006; Thomas et al. 2008). Optical properties vary from glass to glass and sensitivity to the laser should be tested for each sample before analysis by gradually increasing laser power and checking for potential burn marks (Supplementary Figure S1). If samples are embedded in or otherwise held in place by glue or resin it is also important to make sure that they are not fluorescent or Raman active at frequencies within the desired spectral range.

2.2 H₂O quantification

H₂O dissolved in silicate glass produces Raman signal between 2200 and 4000 cm⁻¹ (Figure 2 and 3B) and analysis of the intensity of this H₂O band is the basis for all existing H₂O calibrations. There are two general calibration methods: external and internal. The external method quantifies the re-

lationship between the integrated area (or sometimes height) of Raman H₂O peaks (I_{H_2O}) and glass H₂O contents by regressing known H₂O contents of calibration materials against their measured I_{H_2O} (Behrens et al. 2006; Mercier et al. 2009; Schiavi et al. 2018). The internal method first normalises I_{H_2O} to the integrated area of one or more Raman peaks in the silicate region (I_{Si}) of the analysed sample (Zajacz et al. 2005; Le Losq et al. 2012; Di Genova et al. 2017) and then compares this ratio (I_{H_2O}/I_{Si}) to known H₂O contents in calibration materials. This method increases reproducibility and reduces the effects analytical conditions and instrumental setup (laser power, counting time, etc.) have on the calibration. Additionally, some authors (e.g. Le Losq et al. 2012; Di Genova et al. 2017; Schiavi et al. 2018) correct raw intensities for frequency and temperature dependencies (the Long correction Long 1977; Neuville and Mysen 1996)

2.3 Spectral processing

Since Raman spectra include fluorescent background signal (Figure 2), peak height and area cannot be calculated directly from raw spectra and first require a baseline fitting strategy. This baseline is fitted to areas of the spectrum without peaks (baseline interpolation regions, BIRs) and subsequently extended to the entire spectrum. Various

110 algorithms have been used in the past including linear extrapolation (Zajacz et al. 2005) and inter-
 polations with polynomials (Thomas et al. 2008), cubic splines (Behrens et al. 2006; Di Genova et al.
 115 2017) or smoothing splines (Le Losq et al. 2012). While different algorithms give baselines with different local curvatures, the overall shape is mostly controlled by *BIR* placement (e.g. Di Muro et al. 2009). Where and how many of these should be placed depends on the peak positions and shapes and determining this in a consistent way requires prior knowledge on the parameters that influence spectrum topology. Still, the fact that different procedures have been proposed in recent publications shows that this remains subject to interpretation and is not a straightforward exercise (cf. Le Losq et al. 2012; Di Genova et al. 2017; Schiavi et al. 2018). Another aspect that has to be taken into account is that Raman instrumental setup may also influence *BIR* placement. For instance, gratings with narrower groove spacings have higher spectral resolutions and produce narrower peaks than coarser gratings (e.g. 1800 vs. 150 grooves/mm.), affecting spectrum topologies. Lastly, since background shapes and intensities may even vary within single glasses (Section 4.2), it is important to process and inspect spectra individually.

2.4 Silicate glass spectrum topology

140 The aluminosilicate network of glasses produces Raman peaks in the region 200–1300 cm^{-1} , where the topology is controlled by the structure and composition of the glass (Figure 2; McMillan and Piriou 1982; Schiavi et al. 2018; Giordano et al. 2020). This region is characterised by two main bands between 200–660 cm^{-1} (Figure 3A, low wavenumbers; LW) and 800–1300 cm^{-1} (high wavenumbers; HW), with a minor band often separating the two (medium wavenumbers; MW).

2.4.1 LW band

150 In the silicate network, vibrations of bridging oxygen (BO) part of tetrahedral rings produce peaks with positions between 400 and 660 cm^{-1} (Sharma et al. 1981; McMillan et al. 1994; Neuville et al. 2014). The more tetrahedra are part of these rings, the lower the wavenumber of the produced peak. In pure SiO_2 , BO vibrations in rings with three, four and five or more tetrahedra produce peaks at respectively 660, 485–490 and 440 cm^{-1} (Sharma et al. 1981; Umari et al. 2003). In practice this means that as glasses get more polymerised and the silicate network expands, the envelope of the LW band shifts to lower wavenumbers and its overall intensity increases (Di Genova et al. 2015).

2.4.2 HW band

165 The HW band is made up of a mixture of peaks resulting from stretching of T-O bonds, where T is a tetrahedral, network forming cation (mainly Si^{4+} , Al^{3+} , Ti^{4+} or Fe^{3+}) and O- non-bridging oxygen (NBO, McMillan 1984; Mysen 2003). These stretching units are referred to as Q^n units, where n is the amount of BO and $4 - n$ the amount of NBO the cation is bonded with, meaning a Q^4 unit is fully polymerised. While peak positions also depend on the cation involved (Mercier et al. 2009), they increase to higher wavenumbers as the Q species increase from Q^1 to Q^4 (Neuville et al. 2014). Contrastingly, as molar proportions of depolymerising, network modifying elements like alkalis or alkaline-earths increase, positions of peaks for all Q species shift to lower wavenumbers and their intensities increase (Neuville et al. 2014). The overall result is that the HW envelope of more silica rich, polymerised glasses shifts towards higher wavenumbers (Di Genova et al. 2015).

2.4.3 MW band

185 The MW band is relatively weak in intensity and commonly attributed to Si-O stretching, where peak heights correlate with glass silica content (Ardia et al. 2014; Neuville et al. 2014, and references therein).

2.4.4 H_2O region

190 O-H stretching in OH groups and molecular H_2O produces a broad peak between 2200 and 4000 cm^{-1} (Figure 2 and 3B; Mysen and Virgo 1980; Malfait 2018). This peak is itself a convolution of multiple peaks produced by OH groups with different geometries and as a result has an overall asymmetric shape, where its height and width are proportional to H concentration (Behrens et al. 2006; Le Losq et al. 2012; Schiavi et al. 2018).

2.4.5 Volcanic glasses

200 For volcanic glasses, the combined behaviour of the LW, HW and MW bands means that as melts change in composition from basaltic to rhyolitic compositions, the topology of their Raman spectra undergoes distinct changes (Di Genova et al. 2015; Giordano and Russell 2018). A useful parameter to describe the structural and chemical properties of these melts is NBO/T (NBO divided by the total sum of tetrahedral cations; Mysen 1983), where low values indicate high degrees of polymerisation and high silica contents and vice versa. In basaltic glasses with high NBO/T values the HW band is located at relatively low wavenumbers with high intensities, whereas the LW band is located at relatively high wavenumbers with lower intensities. As NBO/T decreases towards more rhyolitic compositions, the HW band shifts to higher wavenum-

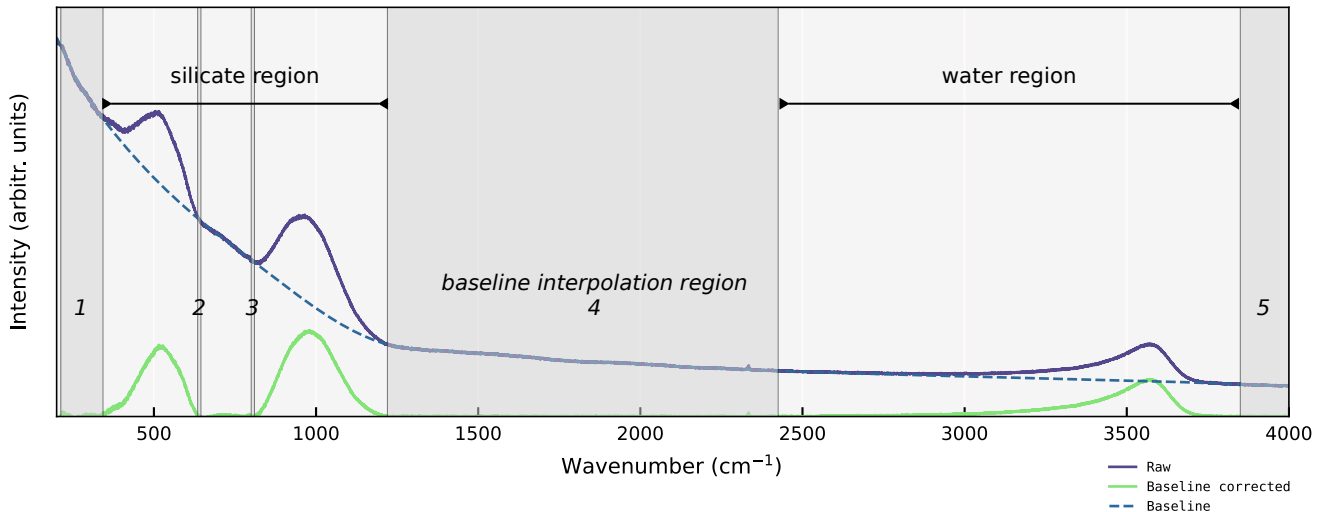


Figure 2: Baseline corrected Raman spectrum of a hydrous silicate glass. The baseline is calculated with five baseline interpolation regions (dark gray bands)

bers and lower intensities, while the LW band increases in intensity and shifts to lower wavenumbers and the MW band becomes more pronounced (Figure 3A). The overall result is that as glasses get compositionally more evolved, the distance between the LW and HW band increases. Additionally, with melt compositional evolution the intensities of the LW and HW bands increase and decrease respectively (i.e. LW/HW increases) and Giordano et al. 2020 found that at NBO/T values below 0.2—0.4 the highest intensity band changes from the HW to the LW band.

3 SPECTRUM PROCESSING WITH SILICH₂O

silicH₂O provides a graphical user interface with all tools necessary for quantifying H₂O in silicate glasses (Figure 1). The implemented algorithms are flexible and allow for different approaches to baseline correction and calibration. Importantly, all parameter settings can be changed interactively and results are shown in real-time. This allows for fast and easy quality control and improves reproducibility compared to command line coding tools. For many calculations, code from the Python library ramCOH (version 1.1.1) is used and users are referred to its documentation (ramcoh.readthedocs.io) for a comprehensive description of the implemented algorithms. If preferred ramCOH can also be used without the silicH₂O interface as a Python command line and scripting tool. Note that silicH₂O is a standalone program, does not require previous installation of Python or any other dependency and is compatible with Mac and Windows operating systems.

3.1 File associations

Spectra are imported from text files with columns for wavenumbers and signal intensities. When data are saved, they are stored together with their calculation settings and results in project files with a .h2o. Project files can hold any number of spectra and can be exchanged and shared between users, encouraging transparent and reproducible data processing. Processed spectra, results (e.g. integrated peak areas, H₂O contents) and settings (e.g. BIR positions) can be exported as tables in .csv format for further analyses or plotting. Alternatively, plots can be saved as is, directly from the interface. Any projects can be used to calculate calibration curves, as long as sample H₂O contents are known. Calibrations are saved individually in .ch20 files and they can be assigned to any project.

3.2 Tools

From the tool bar three main processing options can be selected (Figure 1B): baseline correction (Section 3.2.1), interpolation (Section 3.2.2) and interference subtraction (Section 3.2.3). Interpolation and interference subtraction provide tools for removing unwanted peaks from the glass signal and are optional processing steps, whereas baseline corrections will always be calculated.

3.2.1 Baseline correction

Baselines are calculated by interpolating smoothing cubic splines between BIRs. A minimum of three is needed over the entire spectrum, but otherwise the user is free to add or remove BIRs. BIR location and width are changed by clicking and dragging in the main plot (Figure 1C) or by setting exact boundary values in the settings bar (Figure 1D). Alternatively,

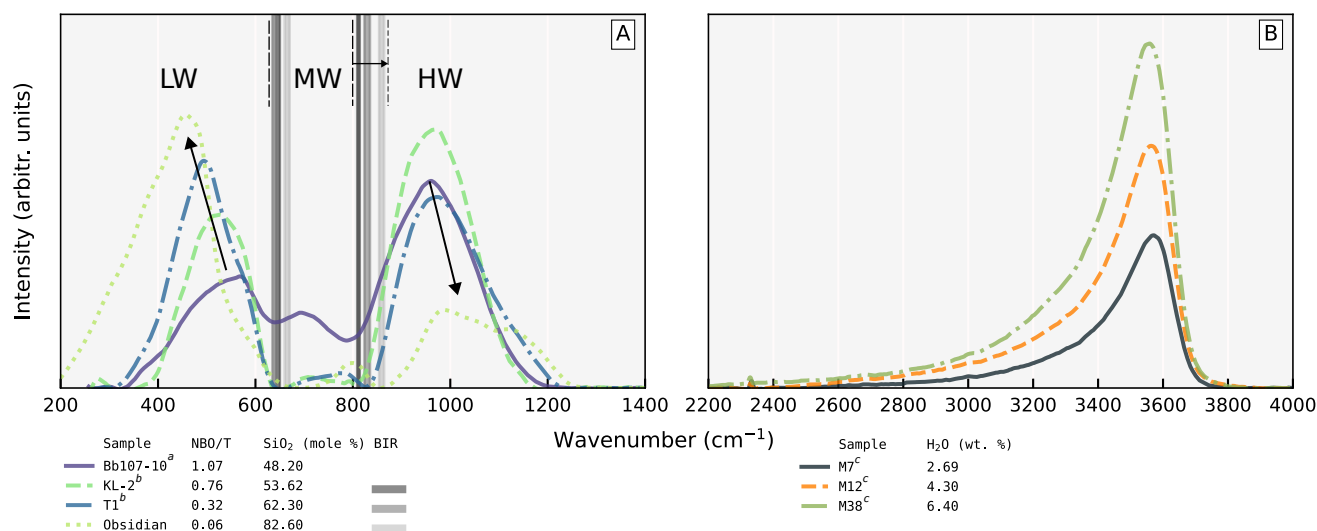


Figure 3: **A** The Raman silicate region of glasses with varying NBO/T (calculated according to Mysen and Virgo 1980). As NBO/T decreases the low wavenumber band (LW) increases in intensity and shifts to lower wavenumbers, while the high wavenumber band (HW) decreases in intensities and shifts to higher wavenumbers (arrows, Section 2.4.5) - suggested BIR positions shift accordingly. Note that sample Bb107-10 has no intermediate BIRs as the LW and HW peaks are close enough together that they overlap and signal in the MW region does not reach the baseline. **B** The Raman H₂O region of hydrous silicate glasses with varying H₂O contents. As H₂O increases, peak intensity and width increase (Section 2.4.4). ^aMédard and Grove 2008, ^bJochum et al. 2006, ^cShishkina et al. 2010

they can be copied and pasted between samples, allowing for quick and easy comparison. Smoothness of the baseline is adjusted with the *smoothing* parameter in the settings menu, which gives linear baselines as it approaches 0, while at higher values ($\gg 1$) the raw data will be followed more closely. By giving the flexibility to adjust BIR location and amount, as well as baseline smoothness, the user is free to implement any of the existing baseline fitting strategies (Section 2.2). Note that baseline corrections are applied to raw spectra; the Long correction (Section 2.2) is currently not implemented as we found that it did not improve results. If needed, Long corrections can still be applied to processed spectra exported from `silicH2O` and `ramCOH` (Section 3) implements a method in Python to do so.

Integrated peak areas of the silicate and H₂O regions and their ratio are recalculated with each parameter change and displayed in the results bar (Figure 1D). The results bar also shows average spectrum noise, which is calculated as two standard deviations on the baseline corrected signal in areas without peaks (i.e. the BIRs set by the user). Some care has to be taken to make sure that BIRs only contain baseline signal, as noise values are only realistic if these regions indeed contain no peaks. Signal-to-noise ratios are then calculated for the silicate and H₂O regions each as *maximum local intensity/noise*. H₂O region signal-to-noise can be used to optimise analytical settings; if this value is below two (i.e. when signal starts to approach the noise level), counting time or laser power should perhaps be increased to get more signal, while at high ratios

counting time could be reduced for more efficient time use. If a calibration file is linked with the active project (Section 3.2.4) H₂O concentration is also recalculated with each parameter change and displayed in the results bar.

3.2.2 Interpolation

Unwanted peaks may appear in glass spectra due to nanocrystalline impurities (e.g. Di Genova et al. 2017) or interference from nearby phases (e.g. resin; Figure 4A Behrens et al. 2006). If these peaks overlap with the silicate or H₂O regions they will affect calculated glass H₂O contents and it is therefore best to remove them. The most straightforward way to do this is to replace the regions with unwanted peaks by interpolations calculated from the rest of the spectrum (Figure 4A). `silicH2O` allows the user to set one or multiple target regions for interpolation by clicking and dragging in an interactive plot. The interpolation algorithm is the same as in the baseline correction tool (Section 3.2.1) and its parameters are set in the same way. Interpolations are shown in real-time as the user adjusts these parameters to best match the results with their estimate of the unaffected signal. Note that interpolation should only be applied when the unwanted peaks are clearly defined and when interpreting the original unaffected signal is straightforward. For spectra with strong interference the unmixing tool is potentially a better suited option (Section 3.2.3).

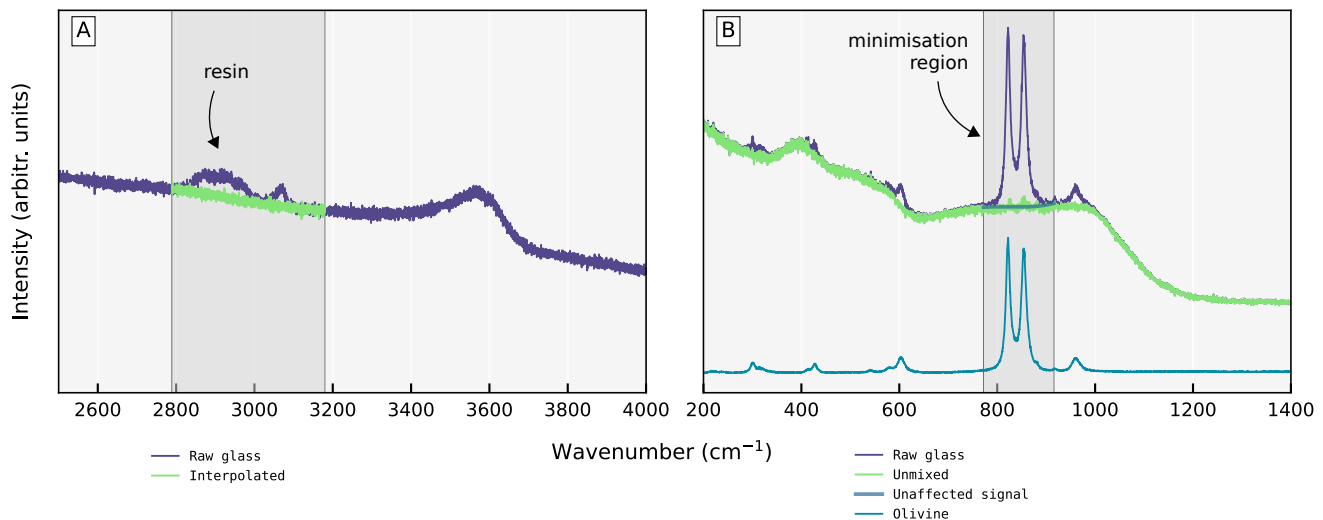


Figure 4: **A** Silicate glass spectrum with unwanted peaks from epoxy resin removed by interpolation (sample PI65-04-03 from van Gerve et al. 2023). **B** Spectrum of a glassy olivine hosted melt inclusion with interfering peaks from the olivine host removed by unmixing and interpolation (sample PI052-03-02 from van Gerve et al. 2023).

3.2.3 Interference subtraction

Signal interference from nearby crystalline phases is common in analyses of crystal hosted melt inclusions (Section 4.1) and may also occur in glass spectra from crystalline experimental charges or glass-dominated volcanic rocks. However, in such cases the interfering phase can also be analysed separately and this makes it possible to numerically unmix the glass and interference signal (Figure 4B).

In SilicH₂O unmixed signal is calculated by subtracting baseline corrected interference signal from the raw, mixed glass signal. Scaling of the interference is numerically optimised by minimising the difference (as root-mean-square error, RMSE) between the unmixed spectrum and a calculated unaffected signal within a region set by the user. Unaffected signal is calculated from a cubic spline interpolation across the minimisation region, which should be narrow and ideally contain the highest interfering peak(s) (Figure 4B). The areas directly left and right adjacent should be free from interference, since these areas strongly impact how unaffected signal is calculated and additional interference peaks present here would give unrealistic results. Finally, the scaled interference is subtracted from the entire spectrum, removing all associated unwanted peaks.

To illustrate: olivine has two main overlapping Raman peaks between 800 and 900 cm⁻¹, as well as a few minor ones (Figure 4B). With such a spectrum the best minimisation region would be one that closely brackets only the major peaks. If there are small discrepancies between peak shapes in the mixed glass signal and the interference itself, large peaks may still leave behind minor unwanted sig-

nal. In such cases interpolation (Section 3.2.2) can be used for additional correction.

Access to these functionalities is provided in the *interference correction* tab of the tool selection bar (Figure 1B). Here, the user first links interference spectra to their corresponding glass spectra by importing them from text files. Baseline corrections of the interference are then set interactively, identical to the procedure for glass spectra (Section 3.2.1). Users have the option to deconvolve the baseline corrected interference before unmixing, which has the added benefit that deconvolutions are noise-free. However, the user should visually compare the deconvoluted and baseline corrected signals and make sure they have a good fit. Further details on deconvolution parameters and settings can be found in the SilicH₂O quickstart guide and the ramCOH code documentation. Lastly, the location and width of the minimisation region is changed by clicking and dragging it in an interactive plot, where the calculated unaffected spectrum is also displayed and updated in real-time.

3.2.4 Calibration

In the calibration menu active projects can be imported and used to calculate calibration curves. The users assigns known H₂O concentrations to each sample and selects which samples should be included in the calibration. Currently, SilicH₂O only supports internal calibration (Section 2.2). However, it is still possible to use results exported from SilicH₂O for external calibration, but this has to be done manually with other software or code (e.g Excel, Python, R). With the internal calibration, linear regressions are calculated in SilicH₂O as:

$$\text{H}_2\text{O} = a + b \times \frac{\text{Area}_{\text{H}_2\text{O}}}{\text{Area}_{\text{Silicate}}} \quad (1)$$

Since the calibration curve is linear, only a limited number of calibration materials is needed in theory, but they should at least cover the full range of expected H_2O contents in the samples to be measured. R^2 , standard estimate of error (SEE) and p-value regression statistics are provided and updated as samples are added or removed from the calibration. In addition to regression statistics, the fitted value for the intercept (a , Equation 1) can be used as a quality check, as this should be approximately zero. Calibration files are saved with `.ch20` extensions and these files can be linked to any project and shared between users. However, it should be kept in mind that calibration curve slopes (b , Equation 1) are specific to each Raman instrument and calibrations should only be applied to spectra obtained with the same instrument. Additionally, calibration curves have different slopes with different spectral resolutions and if gratings with different groove spacings are available on a single Raman instrument, a separate calibration is needed for each grating.

4 REPRODUCIBILITY

Accuracy and precision of results produced with `silicH2O` were tested with a validation dataset of 145 glasses. It contains experiments on basalts and their residual liquids from from Médard and Grove 2008 and Neave et al. 2019 and Azorean basaltic olivine hosted melt inclusions (MI) from van Gerve et al. 2023, under review. They have 45–58 wt.% SiO_2 , NBO/T of 0.42–1.09 wt.% and 0–4.4 wt.% H_2O (see Supplementary Figures S1 and S2). For calibration, a set of 13 experimental glasses with 47–58 wt.% SiO_2 , 0.33–0.84 NBO/T and 0–6.4 wt.% H_2O was used. All hydrous calibration glasses are from Shishkina et al. 2010, with additional dry ones from Jochum et al. 2006 and Duggen et al. 2007. Raman analyses were done at the Department for Earth and Environmental Sciences (KU Leuven), with specifics on instrumental setup, analytical settings and calibration detailed the Supplementary Text. Spectra of all validation samples are provided in the example projects bundled with `silicH2O`

4.1 Accuracy

Raman results are generally within 0.2 wt.% of reference values, with RMSE values on the validation of 0.05–0.08 wt.% (Figure 5 and Supplementary Data). Still, these values are relative to references values (from SIMS and FTIR) and absolute accuracies also depend on their respective accuracies. Validation errors ($\Delta\text{H}_2\text{O}$, *Raman* – *reference* H_2O) are normally distributed and show no systematic

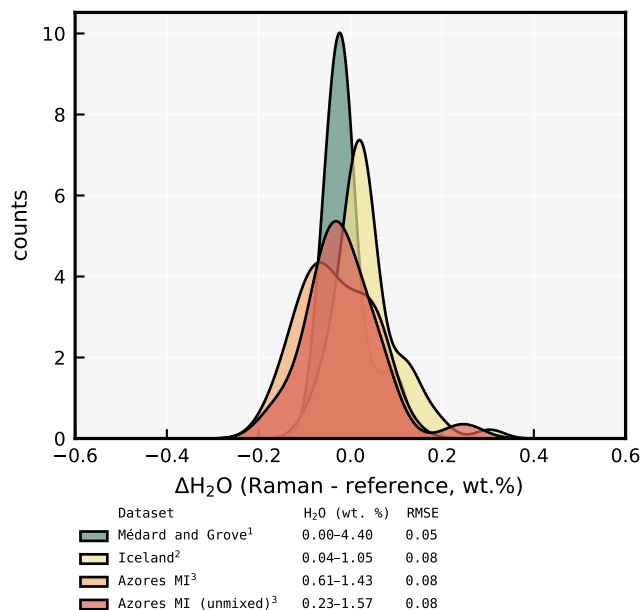


Figure 5: Reference and measured H_2O in validation datasets with basaltic glasses from ¹Médard and Grove 2008, ²Neave et al. 2019 and ³van Gerve et al. 2023, under review. For the Azores melt inclusions part of the data were corrected for interfering host olivine peaks by unmixing (Section 3.2.3)

under- or overestimations. Additionally, $\Delta\text{H}_2\text{O}$ is consistent across varying H_2O contents and glass compositions.

A subset of the olivine hosted melt inclusions showed interference peaks from the crystal host in their Raman spectra (e.g. Figure 4B). However, after unmixing their spectra with the interference correction and interpolation tools in `silicH2O`, validation errors were identical to those in samples free from interference [Azores MI (unmixed), Figure 5]. This shows that with careful data treatment, even samples with unwanted peaks can be used to accurately determine H_2O contents.

4.2 Precision

Analytical precisions were calculated from repeat analyses of a subselection of the calibration materials as one standard deviation (1σ) on their calculated H_2O contents. For all samples precision was below 0.1 wt. %, with no apparent relation with neither H_2O content nor H_2O signal-to-noise ratio (SNR, Table 1, Supplementary Data). Precision therefore mostly depends on data processing consistency and less on signal strength. In practise this means that as long as H_2O peaks are visible (H_2O signal-to-noise > 2), good precisions can be expected from data processed with `silicH2O`. Even single analyses likely give results within 2σ of real values are therefore reliably within 0.2 wt.%

While processing the repeat analyses it was apparent that background signals vary in shape and

sample	H ₂ O ref.	H ₂ O SNR	mean H ₂ O	1 σ	n
N72 ^a	0.32	3.0	0.31	0.03	12
M7 ^b	2.69	17.9	2.64	0.09	9
M12 ^b	3.95	26.3	3.91	0.08	17
M38 ^b	6.4	39.3	6.36	0.06	14

Table 1: 1 σ precisions and signal-to-noise ratios for glasses with various reference H₂O contents (wt. %). ^aDuggen et al. 2007, ^bShishkina et al. 2010

intensity between spectra from single glasses. This means that each spectrum should be processed individually and even analyses from single samples may need different *BIR* positions. This is important since small changes in *BIR* positions may have significant impact on final calculated H₂O contents. *silich₂o* helps address these issues by providing immediate results and constant visual feedback. Furthermore, *BIR* positions can be easily compared between samples by copying and pasting them between each other (see the documentation*)

5 SILICH₂O HIGHLIGHTS

silich₂o makes post-processing and H₂O quantification of silicate glass Raman spectra straightforward and easily accessible by providing an interactive graphical user interface. Quality control is quick and easy as results and processed spectra are shown in real-time. This results in accuracies and precisions mostly within 0.1 wt.% for H₂O contents quantified with calibrations made within *Silich₂O*. Interpolation and interference subtraction algorithms for removing unwanted peaks produce results on par with those from samples where no corrections were needed. Overall, *silich₂o* provides the tools for consistent processing of Raman spectra in order to produce accurate and precise H₂O quantifications.

AUTHOR CONTRIBUTIONS

T. D. van Gerve did the Raman analyses, conceived the idea of developing stand-alone software, wrote code and drafted the manuscript. O. Namur conceived the idea of Raman H₂O calibration and contributed to editing the manuscript.

ACKNOWLEDGEMENTS

This work was supported by a FWO (Research Foundation - Flanders) Odysseus grant to O. Namur. We thank Etienne Médard, David Neave and Renat Almeev for providing samples for validation and calibration.

*<https://silich2o.readthedocs.io/en/latest/>

DATA AVAILABILITY

Silich₂O version 1.0.0 can be downloaded as a release from GitHub[†] and detailed installation and usage instructions are available in its documentation[‡]. The software includes the data reported in Section 4 as example projects. If you want to report a bug, request a new feature or contribute to the code, please open an issue or pull request on GitHub. Supplementary texts and data for calibration, validation and precision tests are available in the Zenodo archive at <https://doi.org/10.5281/zenodo.7808302>.

COPYRIGHT NOTICE

© The Author(s) 2024. This article is distributed under the terms of the Creative Commons Attribution 4.0 International License, which permits unrestricted use, distribution, and reproduction in any medium, provided you give appropriate credit to the original author(s) and the source, provide a link to the Creative Commons license, and indicate if changes were made.

REFERENCES

- Ardia, P., A. Di Muro, D. Giordano, D. Massare, C. Sanchez-Valle, and M. W. Schmidt (2014). “Densification mechanisms of haplogranite glasses as a function of water content and pressure based on density and Raman data”. *Geochimica et Cosmochimica Acta* 138, pages 158–180. DOI: [10.1016/j.gca.2014.03.022](https://doi.org/10.1016/j.gca.2014.03.022).
- Behrens, H., J. Roux, D. R. Neuville, and M. Siemann (2006). “Quantification of dissolved H₂O in silicate glasses using confocal microRaman spectroscopy”. *Chemical Geology* 229(1-3), pages 96–112. DOI: [10.1016/j.chemgeo.2006.01.014](https://doi.org/10.1016/j.chemgeo.2006.01.014).
- Di Genova, D., D. Morgavi, K. U. Hess, D. R. Neuville, N. Borovkov, D. Perugini, and D. B. Dingwell (2015). “Approximate chemical analysis of volcanic glasses using Raman spectroscopy”. *Journal of Raman Spectroscopy* 46(12), pages 1235–1244. DOI: [10.1002/jrs.4751](https://doi.org/10.1002/jrs.4751).
- Di Genova, D., S. Sicola, C. Romano, A. Vona, S. Farnara, and L. Spina (2017). “Effect of iron and nanolites on Raman spectra of volcanic glasses: A reassessment of existing strategies to estimate the water content”. *Chemical Geology* 475, pages 76–86. DOI: [10.1016/j.chemgeo.2017.10.035](https://doi.org/10.1016/j.chemgeo.2017.10.035).
- Di Muro, A., N. Métrich, M. Mercier, D. Giordano, D. Massare, and G. Montagnac (2009). “Micro-Raman determination of iron redox state in dry natural glasses: Application to peralkaline rhyolites and basalts”. *Chemical Geology* 259(1-2), pages 78–88. DOI: [10.1016/j.chemgeo.2008.08.013](https://doi.org/10.1016/j.chemgeo.2008.08.013).

[†]<https://github.com/TDGerve/silich2o>

[‡]<https://silich2o.readthedocs.io/en/latest/>

- Duggen, S., M. Portnyagin, J. Baker, D. Ulfbeck, K. Hoernle, D. Garbe-Schönberg, and N. Grassineau (2007). “Drastic shift in lava geochemistry in the volcanic-front to rear-arc region of the Southern Kamchatkan subduction zone: Evidence for the transition from slab surface dehydration to sediment melting”. *Geochimica et Cosmochimica Acta* 71(2), pages 452–480. DOI: 10.1016/j.gca.2006.09.018.
- Frezzotti, M. L., F. Tecce, and A. Casagli (2012). “Raman spectroscopy for fluid inclusion analysis”. *Journal of Geochemical Exploration* 112, pages 1–20. DOI: 10.1016/j.gexplo.2011.09.009.
- Giordano, D. and J. K. Russell (2018). “Towards a structural model for the viscosity of geological melts”. *Earth and Planetary Science Letters* 501, pages 202–212. DOI: 10.1016/j.epsl.2018.08.031.
- Giordano, D., D. González-García, J. K. Russell, S. Raneri, D. Bersani, L. Fornasini, D. Di Genova, S. Ferrando, M. Kaliwoda, P. P. Lottici, M. Smit, and D. B. Dingwell (2020). “A calibrated database of Raman spectra for natural silicate glasses: implications for modelling melt physical properties”. *Journal of Raman Spectroscopy* 51(9), pages 1822–1838. DOI: 10.1002/jrs.5675.
- Jochum, K. P., B. Stoll, K. Herwig, M. Willbold, A. W. Hofmann, M. Amini, S. Aarburg, W. Abouchami, E. Hellebrand, B. Mocek, I. Raczek, A. Stracke, O. Alard, C. Bouman, S. Becker, M. Dücking, H. Brätz, R. Klemm, D. De Bruin, D. Canil, D. Cornell, C. J. De Hoog, C. Dalpé, L. V. Danyushevsky, A. Eisenhauer, Y. Gao, J. E. Snow, N. Groschopf, D. Günther, C. Latkoczy, M. Guillong, E. H. Hauri, H. E. Höfer, Y. Lahaye, K. Horz, D. E. Jacob, S. A. Kesselmann, A. J. Kent, T. Ludwig, T. Zack, P. R. Mason, A. Meixner, M. Rosner, K. Misawa, B. P. Nash, J. Pfänder, W. R. Premo, W. D. Sun, M. Tiepolo, R. Vannucci, T. Vennemann, D. Wayne, and J. D. Woodhead (2006). “MPI-DING reference glasses for in situ microanalysis: New reference values for element concentrations and isotope ratios”. *Geochimica, Geophysics, Geosystems* 7(2). DOI: 10.1029/2005GC001060.
- Le Losq, C., D. R. Neuville, R. Moretti, and J. Roux (2012). “Determination of water content in silicate glasses using Raman spectrometry: Implications for the study of explosive volcanism”. *American Mineralogist* 97(5-6), pages 779–790. DOI: 10.2138/am.2012.3831.
- Long, D. A. (1977). *Raman Spectroscopy*. New York: MacGraw-Hill, page 267.
- Malfait, W. J. (2018). *Vibrational properties of glasses and melts*. Chapter 5. Elsevier Inc., pages 211–236. ISBN: 9780128113011. DOI: 10.1016/B978-0-12-811301-1.00008-3.
- McMillan, P. F. (1984). “Structural studies of silicate glasses and melts-applications and limitations of Raman spectroscopy.” *American Mineralogist* 69(7-8), pages 622–644.
- McMillan, P. F. and B. Piriou (1982). “The structures and vibrational spectra of crystals and glasses in the silica-alumina system”. *Journal of Non-Crystalline Solids* 53(3), pages 279–298. DOI: 10.1016/0022-3093(82)90086-2.
- McMillan, P. F., B. T. Poe, P. H. Gillet, and B. Reynard (1994). “A study of SiO₂ glass and supercooled liquid to 1950 K via high-temperature Raman spectroscopy”. *Geochimica et Cosmochimica Acta* 58(17), pages 3653–3664. DOI: 10.1016/0016-7037(94)90156-2.
- Médard, E. and T. L. Grove (2008). “The effect of H₂O on the olivine liquidus of basaltic melts: Experiments and thermodynamic models”. *Contributions to Mineralogy and Petrology* 155(4), pages 417–432. DOI: 10.1007/s00410-007-0250-4.
- Mercier, M., A. Di Muro, D. Giordano, N. Métrich, P. Lesne, M. Pichavant, B. Scaillet, R. Clocchiatti, and G. Montagnac (2009). “Influence of glass polymerisation and oxidation on micro-Raman water analysis in aluminosilicate glasses”. *Geochimica et Cosmochimica Acta* 73(1), pages 197–217. DOI: 10.1016/j.gca.2008.09.030.
- Mysen, B. O. (1983). “The structure of silicate melts”. *Ann. Rev. Earth Planet. Sci* 11(1983), pages 75–97. DOI: 10.1090/gsm/146/03.
- (2003). “Physics and chemistry of silicate glasses and melts”. *European Journal of Mineralogy* 15(5), pages 781–802. DOI: 10.1127/0935-1221/2003/0015-0781.
- Mysen, B. O. and D. Virgo (1980). “Solubility mechanisms of H₂O in silicate melts at high pressures and temperatures: a Raman spectroscopic study”. *American Mineralogist* 65, pages 1176–1184.
- Neave, D. A., O. Namur, O. Shorttle, and F. Holtz (2019). “Magmatic evolution biases basaltic records of mantle chemistry towards melts from recycled sources”. *Earth and Planetary Science Letters* 520, pages 199–211. DOI: 10.1016/j.epsl.2019.06.003.
- Neuville, D. R., D. de Ligny, and G. S. Henderson (2014). “Advances in Raman spectroscopy applied to earth and material sciences”. *Spectroscopic Methods in Mineralogy and Materials Sciences* 78, pages 509–541. DOI: 10.2138/rmg.2013.78.13.
- Neuville, D. R. and B. O. Mysen (1996). “Role of aluminium in the silicate network: In situ, high-temperature study of glasses and melts on the join SiO₂-NaAlO₂”. *Geochimica et Cosmochimica Acta* 60(10), pages 1727–1737. DOI: 10.1016/0016-7037(96)00049-X.
- Pasteris, J. D. and O. Beyssac (2020). “Welcome to Raman spectroscopy: Successes, challenges, and pitfalls”. *Elements* 16(2), pages 87–92. DOI: 10.2138/GSELEMENTS.16.2.87.

- 700 Raman, C. V. (1928). “A new radiation”. *Indian journal of Physics*, pages 387–398. DOI: [10.1007/BF03052651](https://doi.org/10.1007/BF03052651).
- Schiavi, F., N. Bolfan-Casanova, A. C. Withers, E. Médard, M. Laumonier, D. Laporte, T. Flaherty, and A. Gómez-Ulla (2018). “Water quantification in silicate glasses by Raman spectroscopy: Correcting for the effects of confocality, density and ferric iron”. *Chemical Geology* 483, pages 312–331. DOI: [10.1016/j.chemgeo.2018.02.036](https://doi.org/10.1016/j.chemgeo.2018.02.036).
- 705
- 710 Sharma, S. K., J. F. Mammone, and M. F. Nicol (1981). “Raman investigation of ring configurations in vitreous silica”. *Nature* 292(5819), pages 140–141. DOI: [10.1038/292140a0](https://doi.org/10.1038/292140a0).
- Shishkina, T. A., R. E. Botcharnikov, F. Holtz, R. R. Almeev, and M. V. Portnyagin (2010). “Solubility of H₂O- and CO₂-bearing fluids in tholeiitic basalts at pressures up to 500MPa”. *Chemical Geology* 277(1-2), pages 115–125. DOI: [10.1016/j.chemgeo.2010.07.014](https://doi.org/10.1016/j.chemgeo.2010.07.014).
- 715
- 720 Thomas, R., N. Metrich, B. Scaillet, V. Kamenetsky, and P. Davidson (2008). “Determination of water in Fe-rich basalt glasses with confocal micro-Raman spectroscopy”. *Z. Geol. Wiss* 36(1-2), pages 31–37.
- 725 Umari, P., X. Gonze, and A. Pasquarello (2003). “Concentration of Small Ring Structures in Vitreous Silica from a First-Principles Analysis of the Raman Spectrum”. *Physical Review Letters* 90(2), page 4. DOI: [10.1103/PhysRevLett.90.027401](https://doi.org/10.1103/PhysRevLett.90.027401).
- 730 van Gerve, T. D., D. A. Neave, P. Wieser, H. Lamadrid, N. Hulsbosch, and O. Namur (2023). “Lower crustal magma storage and differentiation in Ocean Island volcanoes: Integrating 3D imaging with chemical microanalysis of olivine-hosted melt inclusions from Pico (Azores)”. *Journal of Petrology (under review)*.
- 735
- 740 Zajacz, Z., W. Halter, W. J. Malfait, O. Bachmann, R. J. Bodnar, M. M. Hirschmann, C. W. Mandeville, Y. Morizet, O. Müntener, P. Ulmer, and J. D. Webster (2005). “A composition-independent quantitative determination of the water content in silicate glasses and silicate melt inclusions by confocal Raman spectroscopy”. *Contributions to Mineralogy and Petrology* 150(6), pages 631–642. DOI: [10.1007/s00410-005-0040-9](https://doi.org/10.1007/s00410-005-0040-9).
- 745